JMEPEG (2019) 28:5625–5638
https://doi.org/10.1007/s11665-019-04300-y

1059-9495/$19.00

The Effect of Temper, Grain Orientation, and Composition on the Fatigue Properties of Forged Aluminum-Lithium 2195 Alloy

Keren Shen, Mark Timko, Yong-Jun Li, Ray Toal, Nathan Santos, Salim Es-Said, Shonnu Ba Thaung, Luis Guevara, Ryan Riebe, and Omar S. Es-Said

(Submitted February 11, 2019; in revised form July 27, 2019; published online September 4, 2019)

The AA2195 alloy was designed for aerospace applications. Fatigue failures are among the major causes of aircraft failures. However, there exist limited studies on fatigue behavior of forged AA2195 alloy. Samples of AA2195 alloys were taken from an aircraft wheel and an open-die hand-forged billet. A total of 44 aircraft wheel samples and 67 hand-forged samples were tested. Aircraft wheel samples taken from the hub and tubewell were prepared in two tempers: T6 (peak aged) and T8 (cold worked and aged). The hand-forged samples were prepared in three temper conditions (T6, T8-4% strain, and T8-8% strain) and cut in the transverse (T) direction, short-transverse (S) direction and 45° between these directions (ST45). The study revealed that T8 temper, while providing higher strength, showed longer fatigue life compared to T6 temper. The anisotropic behavior of AA2195 hand forgings showed the trend $N_T > N_S > N_{ST45}$. The forged aircraft wheels at different locations and tempers showed similar fatigue life at high stresses. At low stresses, different locations showed significant differences in fatigue lives. The reason may be related to the variance of manufacturing and thermomechanical processes experienced by different locations on a complex-shaped wheel. The AA2195 aircraft wheel samples were also compared with samples taken from a similar aircraft wheel but made of AA2014 alloy. The results revealed that the addition of lithium significantly improved fatigue life.

Keywords aluminum-lithium 2195 alloy, fatigue, forgings

1. Introduction

Al-Li alloys are extensively used in aerospace applications (Ref 1-3), especially in upper and lower wing covers and fuselages (Ref 4). During the last decade, the third-generation Al-Li alloy 2195 (Al-4.0Cu-1.2Li-0.4Mg-0.4Ag-0.12Zr), a member of the Weldalite TM 049 group of alloys, received considerable attention from both scientific communities and the aerospace and military industries (Ref 3, 5, 6). Industrial studies have demonstrated its strengths and advantages: low density and good mechanical properties such as high strength, high stiffness and fracture toughness, good weldability, excellent elevated temperature and cryogenic mechanical properties, high corrosion resistance, and amenability to superplastic forming (Ref 1-3, 7, 8).

Fatigue failure is known to be one of the major issues in aircraft-related crashes (Ref 9, 10). High stiffness, fracture toughness, and good ductility are desired properties of AA2195. Higher ductility can make the material less sensitive to stress concentrations in the cyclic loading, therefore, extending the crack initiation time. This leads to a longer fatigue life at low stress since the major contributing factor of fatigue life is crack initiation (Ref 11). These superior characteristics enabled AA2195 to be a very attractive choice in most weight and stiffness-critical applications, as well as cryogenic applications (Ref 3, 7, 8). It can be considered for applications in large carrier rocket and human spaceflight programs, cryogenic propellant tanks, or large aircraft shells (Ref 1, 5, 12).

Aerospace applications generally require material to be in various forms. For example, forgings are used for propellant and manhole covers, sheets are used for gores, and thick plates of approximately 50 mm thickness are used for the fabrication of propellant tanks made by isogrid machining through pocket milling (Ref 1). Compared to traditional AA2219 and AA2014 alloys that do not contain Li, AA2195 with an adjusted content of Cu and Li has better comprehensive properties such as lower density, ultra-high strength, excellent malleability and weldability, and low anisotropy (Ref 12). Chen et al. (Ref 13) reported that the addition of Cu leads to the formation of T_1 (Al_2CuLi) and θ' (Al_2Cu), which has a positive effect on strengthening the Al-Li alloys. By increasing the Cu/Li ratio, T_1 becomes the primary Cu-bearing phase and possesses a high-volume fraction (Ref 14). In addition, the Cu and Li concentrations and Cu/Li ratio may decide the effectiveness of pre-deformation on precipitates, with the moderate Cu/Li ratio providing the greatest effectiveness (Ref 15).

T_1 (Al_2CuLi) phase is generally considered to be the dominant precipitate and the major strengthening precipitate in

Keren Shen, Nathan Santos, Salim Es-Said, Shonnu Ba Thaung, Luis Guevara, Ryan Riebe, and **Omar S. Es-Said**, Mechanical Engineering Department, Loyola Marymount University, Los Angeles, CA 90045; **Mark Timko**, Weber Metals, Inc., Paramount, CA 90723; **Yong-Jun Li**, MANE Laboratories, College of Science and Engineering, Loyola Marymount University, Los Angeles, CA 90045; and **Ray Toal**, Electrical Engineering and Computer Science Department, Loyola Marymount University, Los Angeles, CA 90045. Contact e-mail: oessaid@lmu.edu.

Al-Cu-Li system (Ref 5, 13, 16-20). T_1 phase is an equilibrium phase, which exhibits a platelet or needle shape about 100 nm in length and 1 nm in thickness, belonging to hexagonal structure (a = 0.497 nm, c = 0.934 nm) (Ref 6, 13). T_1 phase prefers to precipitate on dislocations and grain boundaries, with strong reinforcement effect (Ref 5, 21). The T_1 phase can act as a non-shearable barrier to hinder dislocation motion and slip behavior (Ref 6, 16). It can also retard crack growth inside the grains, leading cracks to grow along the grain boundaries (Ref 6). The ability of T_1 phase to shear depends on its size. Therefore, some researchers consider T_1 as incoherent (Ref 9), while others report it as semi-coherent (Ref 14). Consequently, strengthening would be significantly improved by T_1 phase because of increase in resistance of plastic deformation (Ref 16).

Anisotropic behavior is a major shortcoming in Al-Li alloys because of its critical negative effect on final product quality (Ref 7). The origin of anisotropy results from interactions among (1) crystallographic texture; (2) recrystallization degree and cold deformation; (3) type, distribution and morphology of the main strengthening phases, governed by alloying additions and thermal mechanical processing; and (4) fiber orientation (including grain size and shape, fine grain banding, equilibrium phases, other precipitates in the microstructure, and the alignment of intermediate and coarse intermetallic phases) (Ref 7, 17, 22, 23). Studies revealed that the strong crystallographic textures and texture gradients formed during fabrication of Al-Li alloys were directly responsible for the anisotropy of mechanical properties (Ref 7, 17, 22, 24). Al-Li alloys, with more brass $\{110\}\langle 112\rangle$ component than other Al alloys, exhibit a higher degree of anisotropic behavior since the existence of brass texture component was assumed to be the main reason for anisotropic behavior in these alloys (Ref 7).

El-aty et al. (Ref 7) reported that S $\{123\}\langle 634\rangle$, copper $\{112\}\langle 111\rangle$, and brass $\{110\}\langle 112\rangle$ texture components were observed during the thermomechanical processing of Al and Al-Li to produce sheets, plates, and extruded products. Al-Li alloy products can be controlled by thermomechanical processing and alloy constitution to be either unrecrystallized or recrystallized microstructures (Ref 22). Unrecrystallized flat-rolled products exhibited a strong brass texture (Ref 22, 23). The S and copper texture components were also present, but their intensities were not as high as those of the brass texture component. Recrystallized, flat-rolled products can exhibit strong Cube $\{001\}\langle 100\rangle$ and Goss $\{011\}\langle 100\rangle$ texture components. Typically, the Goss component was higher than Cube in a recrystallized sheet (Ref 22).

Chaturvedi et al. (Ref 19) showed that AA2195-T8 alloy exhibited the highest value of yield strength, fracture toughness, and fatigue threshold in the longitudinal direction and the lowest value at 45° to the rolling direction, due to the presence of the brass-type texture and the relevant cracking characteristics.

Crooks et al. (Ref 24) evaluated the contributions of grain orientation and the presence of T_1 precipitate plates to the in-plane plastic anisotropy of AA2195. Grain orientation, particularly the presence of a strong brass texture, had a pronounced continuous effect on strain localization under 45° loading which produced the lowest yield strength. However, it can be inferred from this study that the strengthening precipitates T_1 had no appreciable effect on the amount of anisotropy. Fatigue process was conditioned by cyclic plastic deformation. Multiple repetitions of even small amounts of plastic deformation led to cumulative damage culminating in failure. Wu et al. (Ref 9) explained that T_1 could be either sheared or bypassed during fracture. The transition between these two mechanisms correlated with the coarsening of the precipitate microstructure and, particularly, with the increase in the T_1 plate thickness. A bypassing mechanism would become dominant when the number and thickness of T_1 precipitates increased.

Kim et al. (Ref 16) showed that the tensile and yield strengths of AA2195-T8 samples, compared to AA2195-T6 samples, were improved by 10% and 28%, respectively. Wang et al. (Ref 21) showed that a T83 (3% pre-stretching) Al-Cu-Li alloy compared to that of T4 (natural aging) and T6 tempers exhibited the highest strength and the lowest ductility, but highest fatigue crack propagation rates due to less crack deflection. Hekmat-Ardakan et al. (Ref 5) showed that the superior strength of the commercially rolled AA2195-T8 was largely attributed to the fine and uniform dispersion of T_1 and θ' precipitates.

In this study, the fatigue life of forged parts was examined. There is very limited data on AA2195 forgings in the open literature. To the best knowledge of the authors, fatigue properties of AA2195 forgings were not studied by other researchers. The samples were taken from an aircraft wheel and a hand-forged plate. Rotating bending fatigue tests were performed since cyclic loading was a good simulation for real-life applications in aerospace.

The objective of this work was to determine the factors influencing the fatigue behavior of AA2195 forgings, including temper, grain orientation direction, and composition. The aircraft wheel samples were prepared in two temper conditions: T6 (peak aged) and T8 (cold worked and aged). The hand-forged specimens were prepared in three temper conditions (T6, T8-4% strain, and T8-8% strain) and cut in the transverse (T) direction, short-transverse (S) direction and 45° between these directions (ST45). AA2195 aircraft wheel samples were also compared with those made from AA2014 alloy to examine the effect of changing the composition.

A total of 164 samples were tested at three different stress levels: 345 MPa (50 ksi), 276 MPa (40 ksi), and 207 MPa (30 ksi). Rotating bending fatigue testing was conducted according to ISO-1143 standards (Ref 25). High cycle fatigue tests (S–N) were generated to analyze the fatigue behavior.

2. Experimental Procedures

2.1 Chemical Composition

The chemical composition of AA2195 alloy used in this study is shown in Table 1, along with the AA2014 alloy chemical composition for comparison. The fatigue properties of both alloys will be compared. The data were provided by Weber Metals, Inc. (Ref 26).

2.2 Specimen Preparation

2.2.1 AA2195 Specimens. Two groups of AA2195 specimens were provided by Weber Metals, Inc. (Ref 26). One group was taken from a closed die-forged aircraft wheel. The other group was cut from a rectangular hand-forged plate. The schematic of the aircraft wheel is presented in Fig. 1. The samples were taken from two locations within this wheel: the hub and the tubewell. The hub is the central part of the wheel,

where the axle is inserted. The specimens were taken in a longitudinal direction from the hub (marked as 7L in the drawing). The other group of specimens were taken in the same direction from the tubewell (shown as 2L in the drawing). These two locations were referred to as 7L and 2L in this study. The samples taken from 7L were prepared in two tempers: T6 and T852. The samples from 2L were only prepared in the T6 temper. Samples prepared in T6 temper were solution-treated then artificially aged. Samples prepared in T852 temper were cold-worked by compression after solution treatment and then artificially aged.

Table 1 Chemical composition of AA2195 and AA2014, provided by Weber Metals, Inc. (Ref 26)

Element	wt.% in AA2195	wt.% in AA2014
Silicon, Si	0.03	0.81
Iron, Fe	0.04	0.26
Copper, Cu	3.81	4.53
Manganese, Mn	0.01	0.88
Magnesium, Mg	0.4	0.62
Chromium, Cr	0	0.02
Nickel, Ni	0	0.03
Zinc, Zn	0	0.12
Titanium, Ti	0.06	0.04
Zirconium, Zr	0.11	0.02
Vanadium, V	0.01	0.02
Lithium, Li	0.9	0
Silver, Ag	0.26	0

A total of 48 samples were taken from the aircraft wheel. Twenty-six samples taken from the tubewell (2L) were prepared in T6 temper. Twenty-two samples were taken from the hub (7L), of which ten of them were prepared in T852 temper and the other 12 in T6 temper. This information is summarized in Table 2.

A total of 83 samples were taken from the rectangular hand-forged plate. The samples were prepared in three different temper conditions: T6, T8-4% strain, and T8-8% strain. At T6 temper, 15 samples were cut in the long transverse (T) direction and 14 samples in the short-transverse (S) direction. At T8 temper with 4% strain, 14 samples were cut in the T direction and eight samples were cut 45° between the T and S directions (ST45) as shown in Fig. 2. At T8 temper with 8% strain, 17 samples were cut in the T direction, 11 samples in the S direction, and four samples in the ST45 direction. This information is summarized in Table 2.

All samples were sectioned and machined into rotating bar bending specimens according to ISO-1143 standards (Ref 25). All samples had a specimen length of 101 mm (4 in), a gage length of 6.35 mm (0.25 in), and an outer diameter of 12.7 mm (0.5 in), as shown in Fig. 3. The specimens were prepared to be of the same size, shape, and tolerance.

All samples were polished to remove any surface micro-cracks that might affect the fatigue behavior. They were polished using three different-sized diamond pastes (9 μm, 6 μm, and 1 μm), with each polishing taking approximately 3 min for a total of 9 min. After polishing, the samples showed a mirror-polished surface with no observable surface scratches.

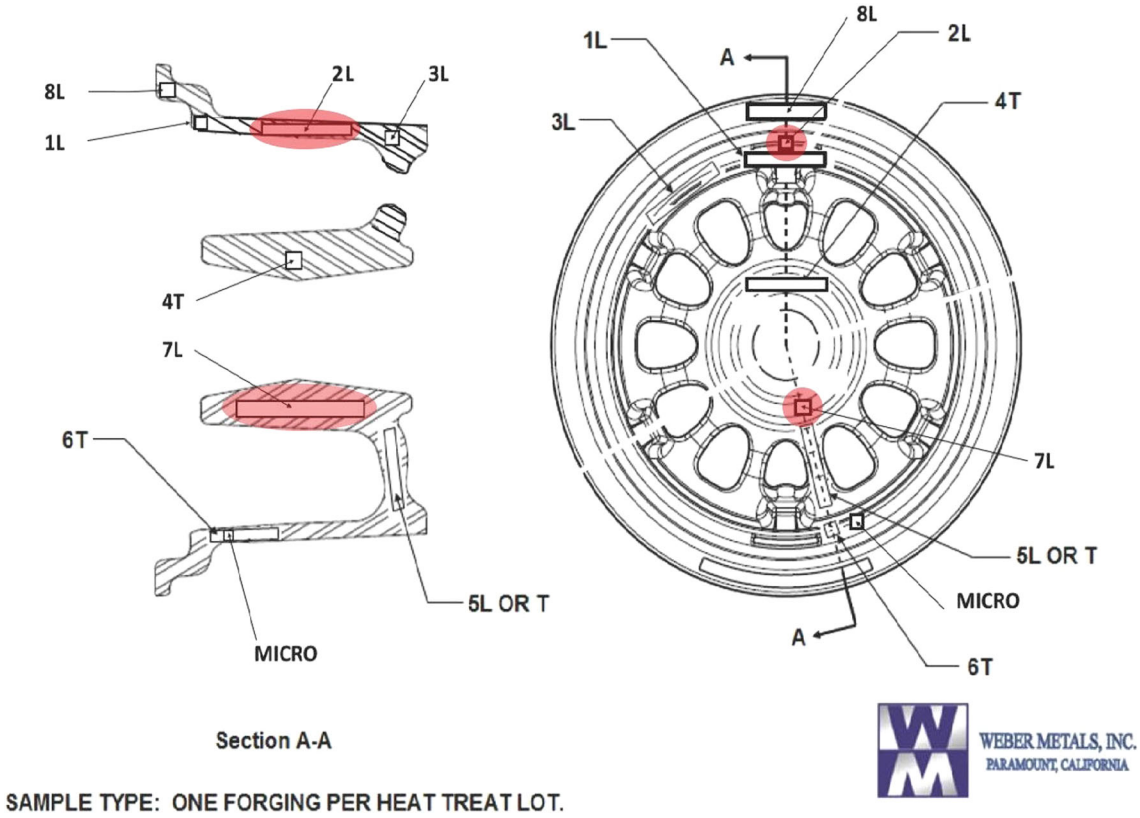

Fig. 1 Location from which the AA2195 specimens were taken from the aircraft wheel, provided by Weber Metals, Inc. (Ref 26)

2.2.2 AA2014 Specimens. A total of 60 specimens made of AA2014 were taken from the same type of aircraft wheel. Ten specimens were cut at each of the six locations, as shown in Table 2 and Fig. 4. The AA2014 samples were machined and polished using the same dimension and procedure as the AA2195 samples to ensure consistency.

2.3 Fatigue Rotating Bending Test

Fatigue tests were conducted according to ISO-1143 standards (Ref 25). Samples were tested using the rotating beam machine model (RBF-200) operating at 7000 rpm and at room temperature 18°C ± 2°C. Each group of specimens were tested at three stress levels: 345 MPa (50 ksi), 276 MPa (40 ksi), and 207 MPa (30 ksi). The stress was converted to moment force using Eq 1. The moment force was used as the applied load for the fatigue tests. Three to five samples were tested under each stress level, depending on the availability of specimens in each group. The division of specimens is shown in Table 3. At full fracture, the cut-off switch turned off the machine and stopped recording the number of cycles.

The moment load was calculated using the formula:

$$M = S\frac{\pi d^3}{32K_t} \quad \text{(Eq 1)}$$

where S, required test stress in MPa (ksi); M, bending moment in N m (lb-ft); D, specimen diameter in mm (inch); and K_t, stress concentration factor (equal to 1 here).

Table 2 List of fatigue specimens and their tempers and directions/locations (marked in asterisk)

Material	Temper	Direction/location*	Total
AA2195 hand forging	T6	T	15
		S	14
	T8 4% strain	T	14
		ST45	8
	T8 8% strain	T	17
		S	11
		ST45	4
AA2195 aircraft wheel	T852	7L*	10
	T6	7L*	12
		2L*	26
AA2014 aircraft wheel	T6	Tube-L*	10
		Hub-L*	10
		Hub-T*	10
		Ring-T*	10
		Tube-45*	10
		Spoke-L*	10

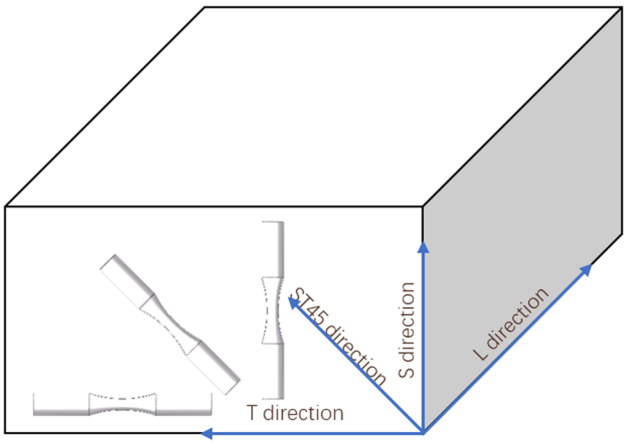

Fig. 2 Schematic of directions in which the specimens were cut from the hand forgings

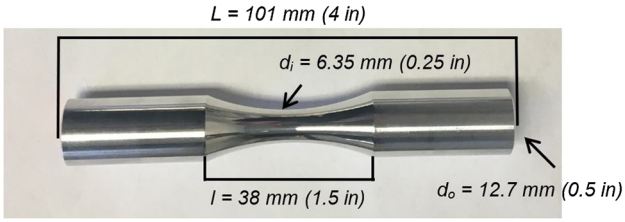

Fig. 3 Dimensions of all fatigue specimens according to ISO-1143 (Ref 25)

2.4 Scanning Electron Microscopy (SEM) and Hardness Measurements

Fractured samples were observed using the FEI Quanta 200 SEM. The magnifications of the fractographs were 30×, 100×, 500×, 1000×, and 5000×. The Rockwell hardness tests were conducted using Wilson/Rockwell Hardness Tester Series 500. The shoulder of each sample was measured ten times. An average measurement was determined for each sample.

3. Results and Discussion

Representative samples with median level or extreme level of fatigue life were chosen and inspected using SEM images and hardness measurements. The S–N curves were generated to analyze the fatigue behavior. Individual groups of hand-forged samples and die-forged aircraft wheel samples were analyzed. The hand-forged and aircraft wheel samples were then compared. Finally, the AA2195 aircraft wheel samples were compared with the AA2014 samples taken from the same type of aircraft wheels heat-treated with the same method, to examine composition difference.

3.1 AA2195 Hand-Forged (HF) Samples Data

Hardness tests were performed to check the strength at each temper. For forged samples, T6 temper had average hardness of 89 RB. T8 temper, with two different strain levels (4% and 8%), showed the same average hardness of 94 RB. The data were consistent, with the standard deviation ranging from 0.67 to 1.29. Different orientations did not show an obvious difference in hardness. With a lower hardness, T6 temper samples showed less strength than T8 temper samples since hardness is proportional to strength.

The fatigue performances between the different orientations at the same temper condition were compared. Then, the fatigue behavior of the different temper conditions at the same orientation was analyzed. S–N curves were generated for the following comparison groups:

(1) At T6 temper, comparing T direction and S direction
(2) At T8-4% temper, comparing T direction and ST45 direction

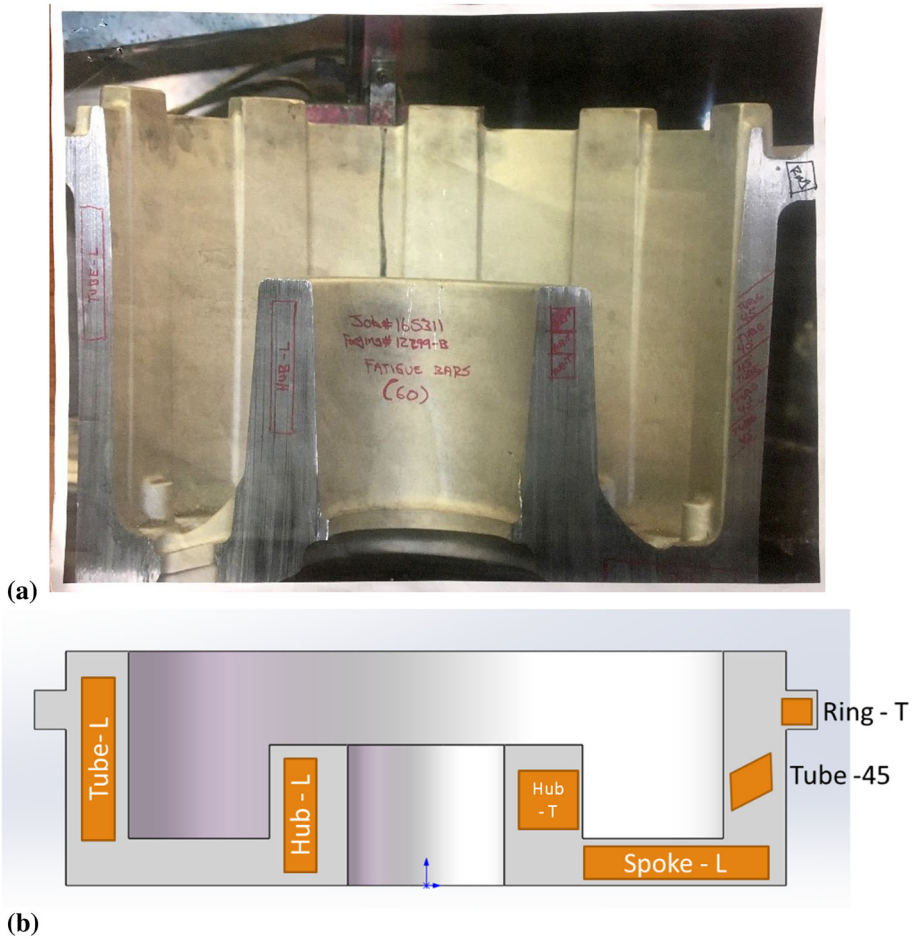

Fig. 4 Aircraft wheel location from which the AA2014 specimens were taken: (a) actual; (b) schematic

Table 3 Number of tests conducted at each stress level

Material	Temper	Direction/location*	Number of samples tested @		
			345 MPa, 50 ksi	276 MPa,40 ksi	207 MPa,30 ksi
AA2195 hand forgings	T6	T	4	4	4
		S	4	4	5
	T8-4% strain	T	4	3	3
		ST45	3	3	...
	T8-8% strain	T	4	4	4
		S	4	3	3
		ST45	4	...	...
AA2195 aircraft wheel	T8	7L*	3	3	4
	T6	7L*	5	5	6
		2L*	5	5	8
AA2014 aircraft wheel	T6	Tube-L*	3	3	3
		Hub-L*	3	3	3
		Hub-T*	3	3	3
		Ring-T*	3	3	3
		Tube-45*	3	3	3
		Spoke-L*	3	3	3

(3) At T8-8% temper, comparing T direction, S direction and ST45 direction
(4) At T direction, comparing T6, T8-4% and T8-8% temper.

Figure 5, 6, 7 and 8 shows S–N curves drawn in a semi-log scale. Data points at all three stresses were plotted along with the power equation used to model the data and show the trendline. Each group had the power equation trendline with R^2

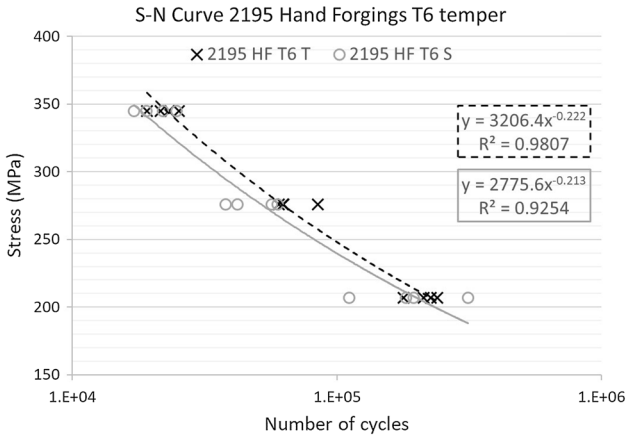

Fig. 5 S–N curve of AA2195 hand forgings at T6 temper, comparing T (dash line) and S (solid line) directions

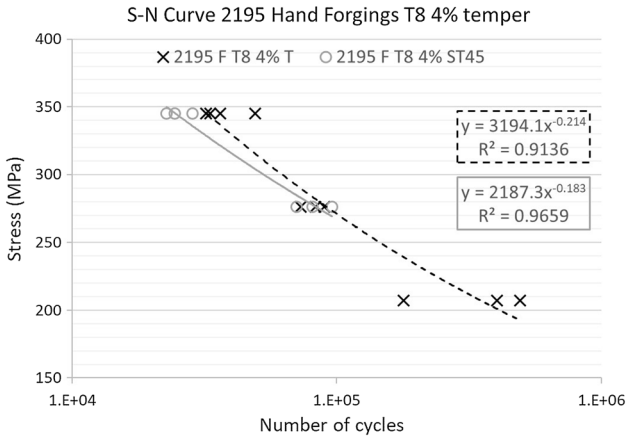

Fig. 6 S–N curve of AA2195 hand forgings at T8-4% temper, comparing T (dash line) and ST45 (solid line) directions

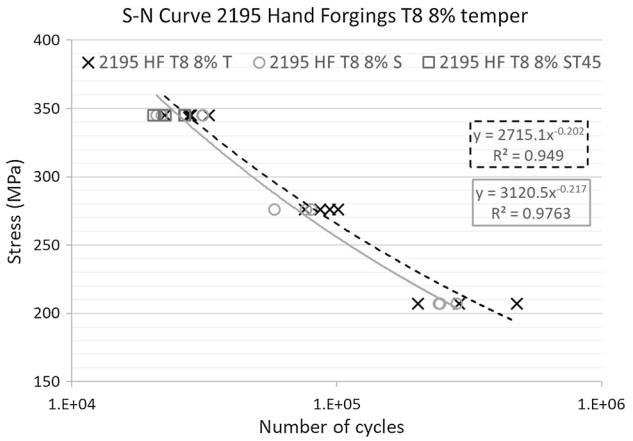

Fig. 7 S–N curve of AA2195 hand forgings at T8-8% temper, comparing T (dash line), S (solid line), and ST45 directions

value greater than 0.9, which indicated a good fit. All trendlines displayed a continuously decreasing slope since there was no endurance limit for Al-Li alloys (Ref 27, 28).

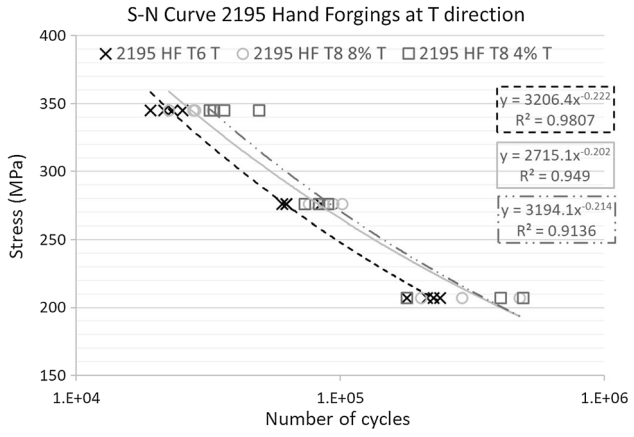

Fig. 8 S–N curve of AA2195 hand forgings at T direction, comparing T6 (dash line), T8-8% (solid line), and T8-4% tempers (dash-dotted line)

(1) HF samples, at T6 temper, comparing T direction and S direction

The S–N curve in Fig. 5 clearly shows that at T6 temper, T direction samples had better fatigue life than S direction samples at all three stress levels. At 345 MPa (50 ksi), the average cycles to failure were 22,275 for T direction and 20,725 for S direction. At 276 MPa (40 ksi), the average cycles to failure were 67,575 cycles for T direction and 49,050 cycles for S direction. At 207 MPa (30 ksi), the average cycles to failure were 214,275 cycles for T direction and 195,620 cycles for S direction. In general, the fatigue performances at T direction were 7% better at 345 MPa (50 ksi), 27% better at 276 MPa (40 ksi), and 8.7% better at 207 MPa (30 ksi) when compared with those at S direction. This is a low level of anisotropy.

(2) HF samples at T8-4% temper, comparing T direction and ST45 direction

Due to a shortage of specimens at ST45 direction, fatigue tests were only performed at 345 MPa (50 ksi) and 276 MPa (40 ksi). The S–N curve showed that at T8-4% temper, T direction samples had better fatigue life than ST45 direction samples at both stress levels. At 345 MPa (50 ksi), T direction samples took an average of 37,750 cycles to fail, while ST45 direction samples took an average of 25,267 cycles (33% fewer). At 276 MPa (40 ksi), the two directions showed nearly the same average fatigue life (only a 0.6% difference). The T direction failed at approximately 82,000 cycles, while the ST45 direction failed at approximately 82,533 cycles. Figure 6 shows that the difference in fatigue life became smaller as stress level decreased. The trend would be improved if more specimens at ST45 direction were available for fatigue testing at 207 MPa (30 ksi).

(3) HF samples at T8-8% temper, comparing T direction, S direction, and ST45 direction

The S–N curves in Fig. 7 clearly show that at T8-8% temper, T direction samples had better fatigue life than S direction samples at all stress levels. Due to a shortage of specimens, fatigue tests were only performed at 345 MPa (50

ksi) for the ST45 direction. As shown in Fig. 7, the number of cycles for the ST45 direction at 345 MPa (50 ksi) was lower than that of the T and S directions, indicating a lower fatigue life at this direction.

The average number of cycles to fail at 345 MPa (50 ksi) for T, S, and ST45 directions was 27,875, 26,325 and 24,125, respectively. The fatigue performance at T direction was 5.9% higher than that of S direction and 15.5% higher than that of ST45 direction. At 276 MPa (40 ksi), samples at T direction, with an average 89,675 cycles of fatigue life, performed 20% better than those at S direction with 71,833 average cycles. At 207 MPa (30 ksi), samples at T direction, with an average 339,450 cycles of fatigue life, performed 24% better than those at S direction with 257,533 average cycles.

(4) HF samples at T direction, comparing T6, T8-8%, and T8-4% temper

In Fig. 8, the S–N curve of T6 temper is consistently lower than the curves of the two T8 temper groups. T8-8% showed lower fatigue life than T8-4% at higher stresses. However, as the stress decreased, the two curves merged together, indicating similar fatigue lives. The average number of cycles for T6 and T8-8% was lower than T8-4% by 41% and 26%, respectively, at 345 MPa (50 ksi). The average fatigue life of T6 was lower than T8-4% temper by 18% at 276 MPa (40 ksi) and by 40% at 207 MPa (30 ksi). The average fatigue life of T8-8% temper was similar to that of T8-4% at lower stress: It was slightly better than T8-4% temper by 8.6% at 276 MPa (40 ksi), and lower by 5.3% at 207 MPa (30 ksi).

The SEM images of specimens from T6 temper in the T direction and S direction are shown in Fig. 9. All specimens show a flat fracture surface with shear lip. However, under SEM, the two directions show significantly different features. S direction samples show clear cleavage steps, indicating a mixed-mode fracture with more brittle features (Ref 29). All three stress levels showed similar fracture type except at 207 MPa (30 ksi) where more dimples were present. T direction samples showed mixed-mode fracture with more dimple-like characteristics. The presence of dimples indicated a high level of ductility (Ref 10). The sub-grains of T direction samples were smaller compared to those of S direction samples. Wu et al. (Ref 9) and Alzubi et al. (Ref 30) both explained that smaller grains leading to increased grain boundary areas can impede the nucleation and the growth of fatigue cracks, thus giving a higher fatigue crack propagation resistance. This could have contributed to the superior fatigue life in T direction.

Specimens from T8-8% and T8-4% groups had very similar fracture surfaces. At the macro-level, all specimens reveal flat fracture surface with shear lip except ST45 specimens, which showed 45° slope. The features in the SEM photographs were similar in appearance at each magnification. The sub-grain sizes were small, and many dimples were observed. The fracture appeared more ductile compared with T6 temper.

The texture of a T6 temper Al-Cu-Li alloy was mainly composed of Goss and a little of Cube; T8 temper Al-Cu-Li alloys were reported to be predominantly composed of brass texture with the existence of copper and reduced Goss texture (Ref 9, 19, 21, 31). Wang et al. (Ref 21) showed 3% pre-stretching of T83 temper resulted in stronger brass $\{110\}\langle112\rangle$ and facilitated T_1 precipitation.

Dislocations had to bypass T_1 precipitates with thickness greater than a critical value, and a large number of dislocations would accumulate at the tip of the crack and result in stress concentration along the grain boundaries. Fatigue cracking tends to nucleate at those stress concentration sites, facilitating rapid fatigue crack propagation. Goss $\{011\}\langle100\rangle$ grains could induce fatigue crack deflection and were thus responsible for the enhanced fatigue crack propagation (FCP) resistance (Ref 9, 21). The dominance of Goss texture in a T6 temper Al-Cu-Li alloy was reported to be responsible for the low FCP rate, as the fatigue crack was deflected to different angles with the existence of secondary cracks (Ref 21).

Previous results revealed that brass $\{110\}\langle112\rangle$ grains had low FCP resistance due to the negative inhibition of small twist angle component boundaries to fatigue crack growth (Ref 9). Brass texture intensity is associated closely with T_1 precipitates. T_1 precipitates retarded the reversible dislocation slipping in the plastic zone ahead of the crack tip, leading to less crack deflection and greater FCP rate (Ref 21). A T83 temper Al-Cu-Li alloy, with strong brass T_1 precipitation, showed degraded FCP resistance due to less crack deflection and less secondary cracks (Ref 21). However, an Al-Cu-Li-T87 alloy tested by Wu et al. (Ref 9) showed induction of crack deflection due to the relatively large twist angle of grain boundaries between brass grains and neighboring grains when considerable T_1 precipitates were observed. Further work was needed to investigate the relationship of T_1 precipitates and brass grains on FCP in Al-Cu-Li alloys. However, the results of this study clearly indicated that the overall fatigue life was higher in the T8 temper as compared to the T6 temper.

For the anisotropic behavior in fatigue life of hand-forged samples, T6 temper in T direction samples performed better than S direction samples in fatigue performance ($N_T > N_S$); T8-8% temper in T direction performed better than S direction, and both were better than ST45 direction ($N_T > N_S > N_{ST45}$); T8-4% temper in T direction performed better than ST45 direction ($N_T > N_{ST45}$). The result that 45° had the lowest fatigue life was consistent with results shown in other works (Ref 9, 17, 19, 24, 32). The comparison is listed in Table 4.

The T and S direction samples of T6 temper showed different fracture types under SEM. The S direction showed more brittle cleavage, while the T direction showed more ductile dimple-like characteristic and smaller sub-grain size. The difference was in accord with the result shown in the S–N curve. Though T6 temper showed clear differences between different directions at the microscopic level, the SEM images showed very similar fracture types for all groups under the two T8 tempers.

Several researchers explained that the main contribution to anisotropy was the texture effect (Ref 6, 17, 22, 24). Several studies showed that T8 temper Al-Cu-Li alloys were dominated by brass texture $\{110\}\langle112\rangle$, while T6 showed more Goss (Ref 9, 19, 21, 22, 31). It was concluded that the more brass $\{110\}\langle112\rangle$ component present, the higher degree of anisotropic behavior would be experienced by the Al-Li alloys, because brass texture, with small twist angle component boundaries, was not good at crack deflection (Ref 9). Thus, it was expected that T8 temper should experience more anisotropic behavior than T6 temper. However, the average percentage difference between T and S directions at T6 temper is 14.2% and at T8-8% temper the difference is 16.5%. Thus, T8-8% temper did not show significantly worse anisotropic behavior than T6 temper in this study. Forging, being more random and multi-directional in deformation (hot work), seems to have less anisotropy compared to rolling and extrusion in one direction.

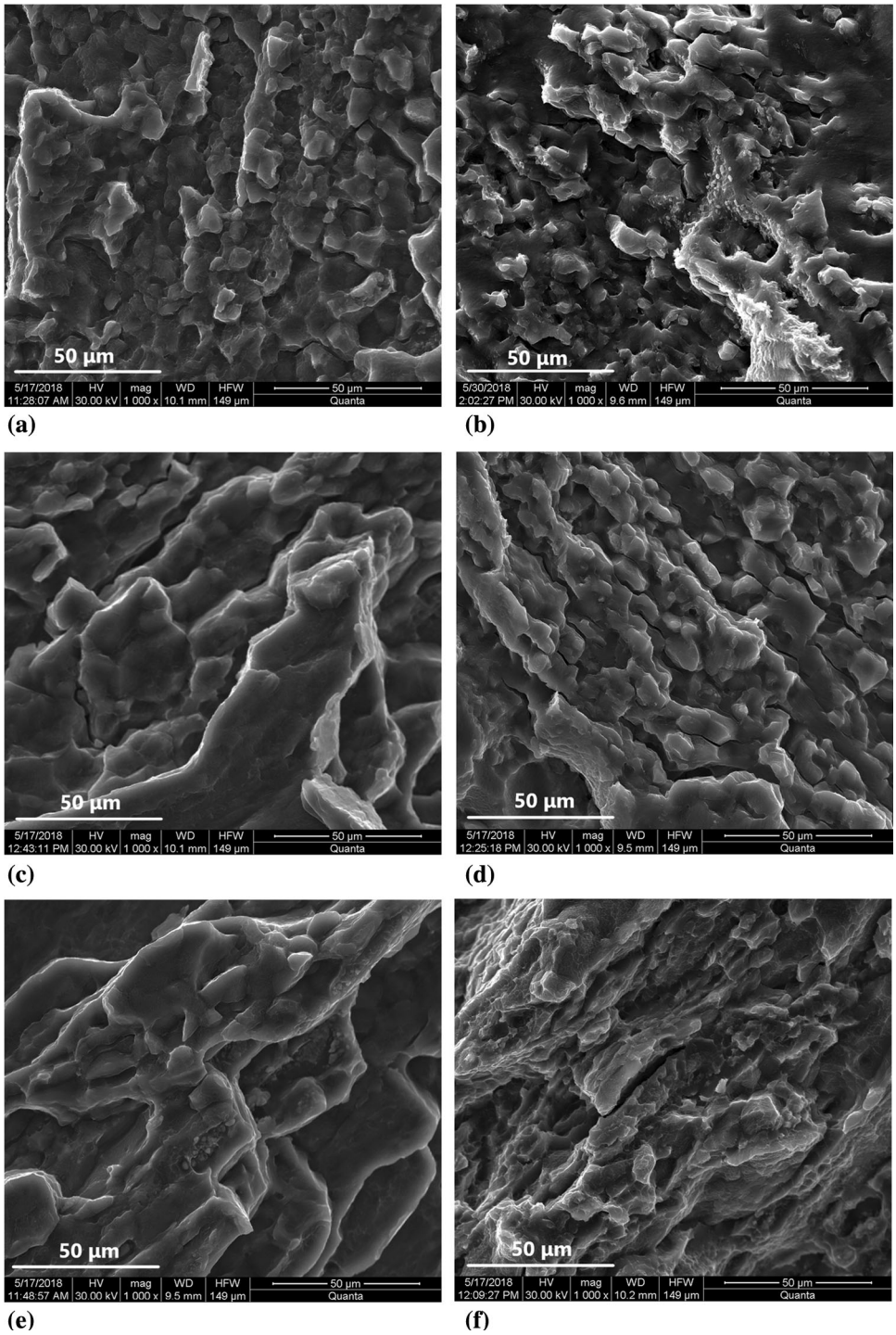

Fig. 9 SEM images at ×1000 magnification for T6 S direction of aluminum lithium 2195 at (a) 207 MPa, (c) 276 MPa, (e) 345 MPa and T6 T direction of aluminum lithium 2195 at (b) 207 MPa, (d) 276 MPa, (f) 345 MPa

Table 4 Anisotropic behavior at each temper of aluminum lithium 2195

Temper	Fatigue life
T6	$N_T > N_S$
T8-4%	$N_T > N_{ST45}$
T8-8%	$N_T > N_S > N_S$

When comparing the temper in sample direction T, hand-forged samples show that T8 tempers had better fatigue life than T6 temper; these results were in accord with Gazizov et al. (Ref 33) and Xia et al. (Ref 34). Wu et al. (Ref 9) indicated that brass texture with a large amount of small-size T_1 can have large twist angle, inducing crack deflection and promoting planar slip, leading to a good resistance to fatigue crack growth.

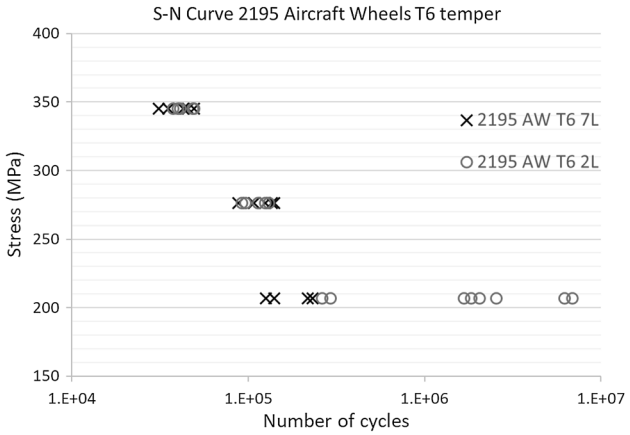

Fig. 10 S–N curve of AA2195 aircraft wheel samples at T6 temper, at locations 7L and 2L

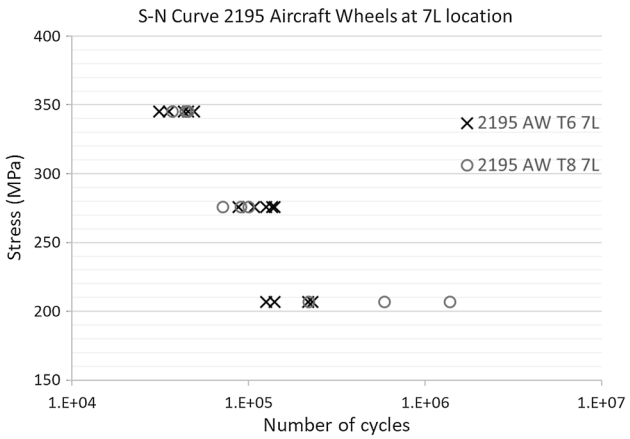

Fig. 11 S–N curve of AA2195 aircraft wheel samples at location 7L, at T6 and T8 tempers

This could be one possible reason why T8 temper has longer fatigue life than T6 temper.

The 4% strain and 8% strain for T8 temper showed similar fatigue life at 276 MPa (40 ksi) and 207 MPa (30 ksi); however, T8-4% strain showed significantly better fatigue life at 345 MPa (50 ksi). The similar fatigue life of T8-4% and T8-8% shown in this study agrees with Rodgers et al. (Ref 35) and Li et al. (Ref 15). Both revealed the lack of effectiveness of pre-strain at higher strain levels (5-6%). The lower fatigue life of T8-8% samples compared with T8-4% at 345 MPa (50 ksi) could be due to the fact that, at high stress levels, samples with more strain were prone to having more micro-cracks, leading to poor crack resistance as explained by Es-Said et al. (Ref 17).

In this study, the results supported a positive correlation between strength and fatigue life. The T8-8% and T8-4% temper samples showing similar fatigue behavior had the same hardness, while they both have longer fatigue life and higher hardness than T6 temper samples. The conventional manufacturing route for aluminum aerospace plates involves a stretching operation after solution heat treatment to relieve the large residual stresses developed when quenching, during which the material is typically plastically strained between 2 and 5% (Ref 35). This pre-deformation had an evident effect on the precipitation process (Ref 18). A small pre-deformation prior to artificial aging can produce a uniform distribution of dislocations within the matrix, which acted as heterogeneous nucleation sites for the T_1 phase. This promoted the nucleation of a fine homogeneous distribution of the T_1 phase throughout the material during artificial aging (Ref 2, 5, 18, 35, 36). The number of T8 T_1 precipitates can be increased by approximately two orders of magnitude compared to T6 with no cold work (Ref 22). The optimum distribution of T_1 precipitates generated by this pre-deformation was highly beneficial to the strength and fracture toughness for the third-generation Al-Li products (Ref 15, 22, 35).

Xia et al. (Ref 34) indicated that T8 temper with 4% pre-stretching can improve the fatigue strength and fatigue life under 300 MPa (43.5 ksi) as compared to T6 temper, for a 2A12 aluminum alloy. Extensive studies were done on AA2195-T8, which included the cold working prior to aging. All showed the existence of a mass of uniformly distributed T_1 precipitates (Ref 2, 5, 6, 19, 21). Uniformly distributed T_1 phase in AA2195-T8 promoted homogeneous slip, in contrast to other Al-Li alloys that exhibited localized slip mechanisms. T_1 precipitate was considered responsible for the relatively good strength and fracture toughness properties of AA2195-T8 when compared to other Al-Li alloys (Ref 6).

In theory, Laird's (Ref 37) crack tip plastic blunting model supports the notion that higher yield strength leads to a lower fatigue crack propagation rate (Ref 10). The results are in accord with the results of other researchers. Gazizov et al. (Ref 33) indicated that for AA2139, samples under T840 condition had improved yield strength (YS)/ultimate tensile strength (UTS) and slightly longer fatigue life than those under T6 temper. Tian et al. (Ref 29) tested A319 castings and indicated that peak-aged specimens with higher yield and tensile strengths had longer fatigue life than that of the over-aged samples. Kermanidis et al. (Ref 38) showed T3/T8 welds with higher hardness value presented better fatigue life than T4 welds for 6156 aluminum alloys.

3.2 AA2195 Aircraft Wheel (AW) Sample Data

The fatigue test data of AA2195 aircraft wheel samples (AW samples) were determined at three different stress levels. The samples were grouped based on their location: T6 temper at location 7L (T67L), T6 temper at location 2L (T62L), and T8 temper at location 7L (T87L) as shown in Table 2. The average, median, standard deviation, and Weibull modulus for each group were calculated.

For AW samples, at 345 MPa (50 ksi), the three groups (T67L, T87L, and T62L) had very similar fatigue lives with average and median levels around 40,000 cycles. At 276 MPa (40 ksi), the T67L and T62L groups were still similar, with the T67L samples only 6.8% higher on average than T62L samples. The T87L group showed lower fatigue life at this stress; it was 27% lower compared with T67L. The three groups showed large differences in fatigue life at 207 MPa (30 ksi). The T62L group had an average life notably higher than the other two groups by an order of magnitude, indicating that difference in locations can have a significant effect on fatigue life. At the 7L location, the average fatigue life of T8 temper was more than double that of T6 temper.

The Weibull modulus of fatigue data of the AW samples ranged from 5.41 to 8.30 at 345 MPa (50 ksi), from 5.26 to 6.49 at 276 MPa (40 ksi), and from 0.85 to 2.52 at 207 MPa (30 ksi). The Weibull modulus clearly showed a decreasing

trend as the stress decreased, indicating that the fatigue data became more scattered at lower stress levels (Ref 28). The same trend was revealed by Alzubi et al. (Ref 30).

Hardness testing was performed on representative specimens to check the strength at each temper. The average hardness for aircraft wheel samples was approximately 90–91 RB as shown in Table 5. The standard deviation values of the three groups (0.85, 0.45, and 0.24) were below 1, indicating good consistency of data.

The tensile strength, yield strength, and percent elongation of AW samples were provided by Weber Metals, Inc. (Ref 26) and are presented in Table 5. At location 7L, the T8 temper showed a higher YS/UTS than the T6 temper. In the T6 sample, location 2L (tubewell) exhibited higher YS/UTS than location 7L (hub). Here, the hardness data did not reflect the difference of YS/UTS between each group.

The S–N curves were drawn in a semi-log scale, comparing T67L with T87L, and T67L with T62L, for all three stresses. The power equation was used to model the data; however, the R^2 value was very low, indicating that the trendline was not a good fit. Thus, the power equation trendline was removed from the graphs.

Figure 10 shows a general trend that location 2L (tubewell) has better fatigue life than 7L (hub) in the T6 temper. The difference was more obvious at low stress levels. The actual data indicated similar fatigue life at high stress levels: The difference between average fatigue of T67L and T62L was only 5.8% and 6.7% at 345 MPa (50 ksi) and 276 MPa (40 ksi), respectively. The distinctive difference appeared at 207 MPa (30 ksi), where the fatigue life of location 2L was an order of magnitude greater than 7L. Because the fatigue life was dominated by the initiation process at this low stress (Ref 11, 27, 30), it was determined that it was more difficult to initiate cracks at location 2L at low stress.

Comparison between T6 and T8 temper at location 7L is shown in Fig. 11. The graph shows that T8 temper had longer fatigue life in general; however, T6 temper stood out at median stress level. The average data indicated T87L was 3.2% higher than T67L at 345 MPa (50 ksi), 27% lower than that at 276 MPa (40 ksi), and 189% higher than that at 207 MPa (30 ksi). It remains to be understood why T67L had excellent fatigue performance at 276 MPa (40 ksi).

The three groups of AW samples at different locations and different tempers exhibited similar fatigue life (approximately 40,000 cycles) at 345 MPa (50 ksi). The two groups at location 7L showed similar fractured surfaces. They both contained dimples, cleavage planes, and micro-cracks, indicating a mixed mode of ductile–brittle fracture. The samples at 2L showed an oblique image because of its inclined fracture surface. The SEM photograph showed a mixed-mode fracture and a dominance of striations, indicating the crack propagation path. Minor dimples and micro-cracks were also visible.

SEM photographs of specimens tested at 276 MPa (40 ksi) level were examined to study the outstanding behavior of T67L. The comparison is shown in Fig. 12. At low magnification, all three specimens showed similar mixed-mode ductile–brittle fracture with more obvious cleavage layers. At higher magnification (1000×), the T67L sample with longer fatigue life showed more sheared dimples. The T62L sample showed a large crack, and the T87L sample had more micro-cracks. These cracks may be the reason for the relatively short fatigue life of these two groups at 276 MPa (40 ksi).

The difference in fatigue life between all three groups at 207 MPa (30 ksi) was the largest. The photographs of fractured surfaces all showed a shear lip, indicating ductile shear fracture. SEM photographs showed mixed-mode fracture for all samples. T62L samples, with the longest fatigue life, showed slightly more dimples.

When studying the 7L and 2L locations at temper T6, similar fatigue life at high and median level stresses was observed. However, the fatigue life of T62L was one order of magnitude better than T67L at 207 MPa (30 ksi). The difference in mechanical properties of these two locations may be caused by the variance in manufacturing process. The hub (7L) is thicker than the tubewell (2L). In addition, the hub is located more toward the center of the wheel. For these two reasons, the hub gets less hot work than the tubewell. This may lead to larger grain sizes at the hub location, which cannot deflect cracks as well as small grains, thus leading to shorter fatigue life.

Comparing T8 temper and T6 temper at location 7L, T8 showed better fatigue life at 345 MPa (50 ksi) and 207 MPa (30 ksi), yet lower life at 276 MPa (40 ksi). In general, the pre-stretching improved the strength. However, compressing a complex-shaped aircraft wheel was not as uniform as compared to compressing a rectangular hand forging. The variance in pre-deformation, affecting texture and size and distribution of T_1 precipitates, could differ the fatigue life performance (Ref 9, 15). T8 samples tested at 276 MPa (40 ksi) may be from bad locations of pre-deformation, thus lowering fatigue life.

Both T87L and T62L groups showed better yield and tensile strength than T67L as listed in Table 5. The general trend was that T87L and T62L, with higher strength, gave better fatigue life. The positive proportional relationship between strength and fatigue life (Ref 9, 10) was revealed again by aircraft wheel samples such as the hand-forged samples discussed earlier. The existence of micro-cracks could be the reason for shorter fatigue life at 276 MPa (40 ksi).

Table 5 Comparison of mechanical properties of aircraft wheel samples of select group (Ref 26)

Material	Group	Tensile, ksi	Tensile, MPa	Yield, ksi	Yield, MPa	Elongation, %	Hardness, RB
AA2195	T8 7L	80.1	552.3	71.1	490.2	8	91
	T6 7L	76.3	526.1	64.7	446.1	12	90
	T6 2L	84.9	585.4	76.2	525.4	8	90
AA2014	Tube-L (T6 2L)	72.9	502.6	66.2	456.4	11	82.5

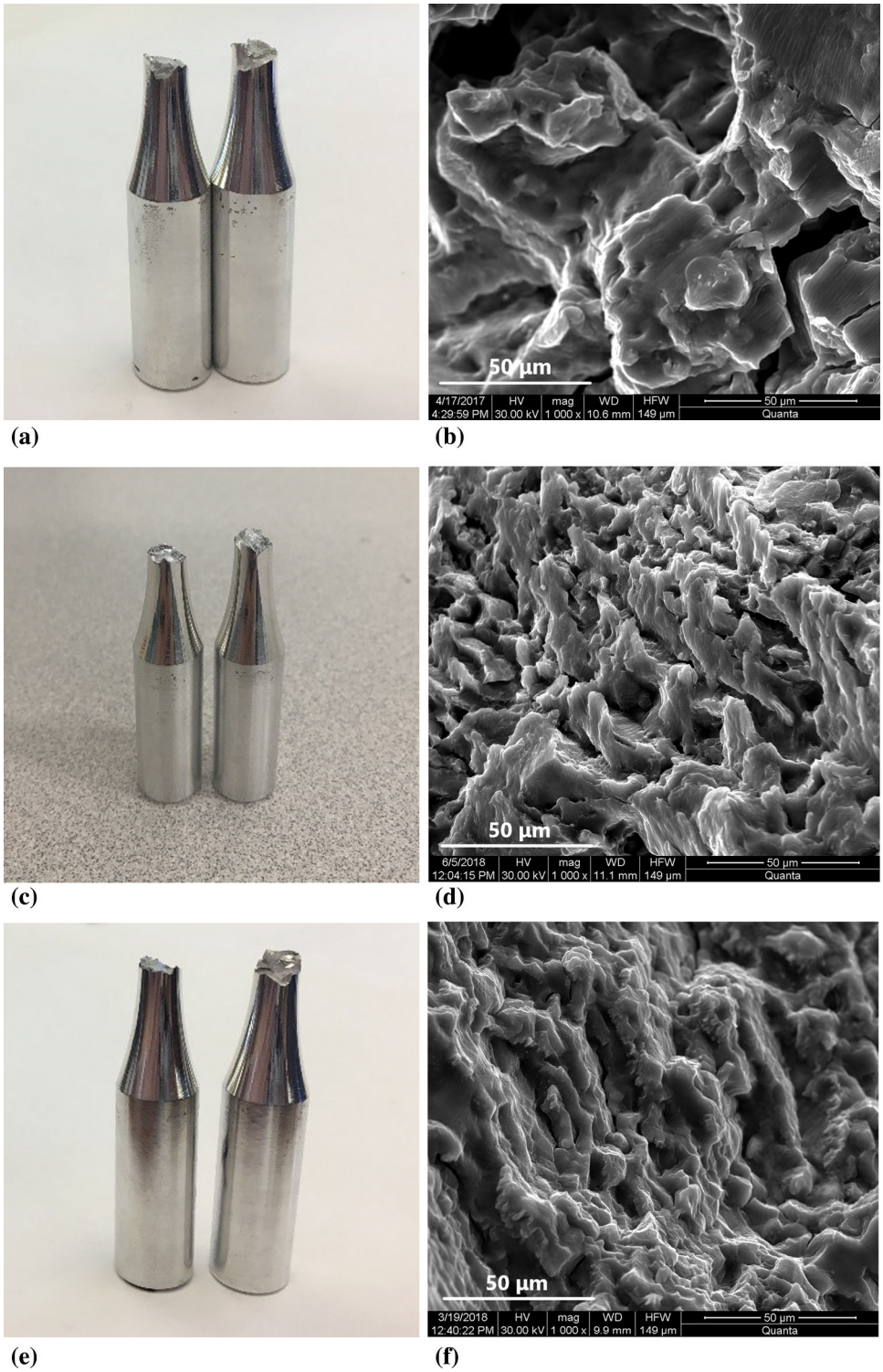

Fig. 12 Photographs of fracture surface and SEM images of aluminum lithium 2195 at ×1000 magnification at 276 MPa (40 ksi), (a, b) T62L; (c, d) T67L; (e, f) T87L

3.3 Comparing Aircraft Wheel Samples Versus Hand-Forged Samples

The close die-forged aircraft wheel (AW) samples and hand-forged (HF) samples showed similar range of variance in fatigue data at high stresses: The Weibull moduli ranged from 4 to 9. At lower stress level, fatigue occurs at a wider range of cycles as most of the Weibull moduli was below 3, but the data from the hand-forged samples, with two groups showing Weibull moduli greater than 7, were more consistent than that of aircraft wheel samples. The cause for extreme data points can be due to the physical condition of the specimen when extracted from different parts with varying hot deformation percentages.

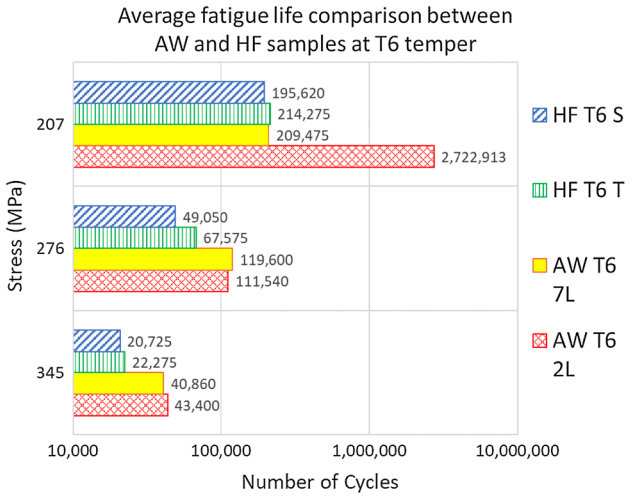

Fig. 13 Average fatigue life of T6 temper of aluminum lithium 2195

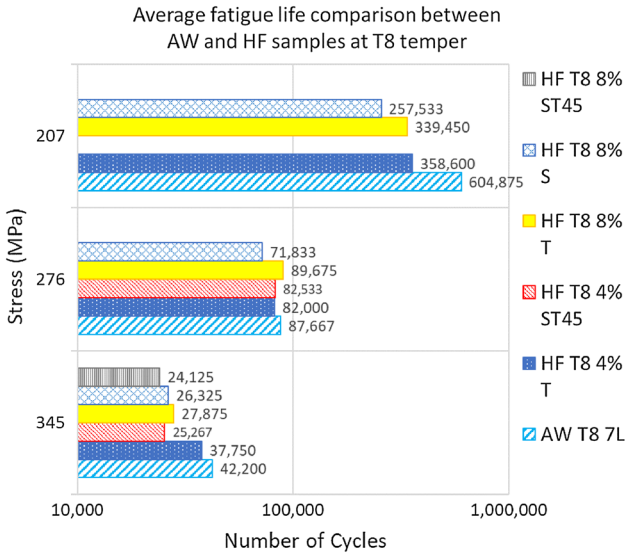

Fig. 14 Average fatigue life of T8 temper of aluminum lithium 2195

The T6 temper HF specimens had lower hardness than T6 temper AW specimens. However, the T8 temper HF specimens, with both 4% and 8% strain, had higher hardness than T8 temper AW specimens. As shown in Fig. 13, the average fatigue life of AW groups at T6 temper was apparently higher than HF groups at 345 MPa (50 ksi) and 276 MPa (40 ksi). At 207 MPa (30 ksi), the differences became much smaller. However, AW location 2L showed significantly higher fatigue life. Figure 14 shows the difference of average fatigue life between AW and HF groups at T8 tempers. AW samples generally showed higher fatigue life than HF samples, except at 276 MPa (40 ksi) where the values were similar. SEM photographs indicated that all samples were presenting a mixed mode, but AW samples were generally more ductile.

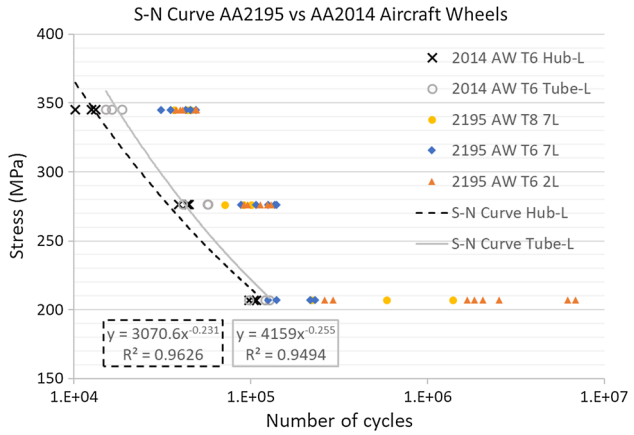

Fig. 15 S–N curve of AA2014 with comparison to AA2195 aircraft wheel sample data

Die-forged aircraft wheel samples generally showed better fatigue life than hand-forged samples. A possible reason could be that the die forging process had more hot deformation ($>$ 90%) compared to the hand forging process (80%). More hot work reduces the size of grains and increases the grain boundaries, which results in a longer fatigue life (Ref 30).

3.4 Comparing Aircraft Wheel Samples Made of AA2195 Versus AA2014

The AA2195 aircraft wheel samples were compared with AA2014 samples taken from a similar location in the same type of wheels. The average, median, standard deviation, and Weibull slope values were obtained using fatigue test data. Specimens cut from the tubewell in the longitudinal direction (Tube-L) were compared to AA2195 AW samples at location 2L. Specimens cut from the hub in the longitudinal direction (Hub-L) were compared to AA2195 AW samples located at 7L. The data were used to generate S–N curves for AA2014 samples and compared with AA2195 samples data, as shown in Fig. 15.

The S–N curves in Fig. 15 show clearly that AA2195 samples had better fatigue life than AA2014 samples at all stresses. The fatigue life of AA2195 AW samples was more than double of the fatigue life of AA2014 samples. AA2014 samples also showed better fatigue life of Tube-L (2L), compared with Hub-L (7L). This matched with the result shown with AA2195 samples.

The SEM photographs of AA2014 specimens show similar fracture type at all stresses. The SEM photograph shows a mixed-mode fracture type; however, it appears more brittle. The SEM images were consistent with S–N curve results, indicating better fatigue life for AA2195 aircraft wheel samples.

The existence of Li in AA2195 could be the reason for better fatigue performance (Ref 7, 22). The addition of Li leads to the formation of T_1 phase, which can prevent the planar slip and retard the nucleation of fatigue cracks, thus improving the fatigue life (Ref 7).

Mechanical properties of AA2014 aircraft wheel samples taken from location Tube-L (2L) were provided by Weber

Metals, Inc. (Ref 26). The data were compared with AA2195 samples taken from the same location, as shown in Table 5. AA2014 had lower tensile strength and lower yield strength than AA2195. AA2195, with higher strength, showed better fatigue life than AA2014. The relationship between strength and fatigue life was verified again.

4. Conclusions

The following conclusions are drawn:

1. Fatigue life increases as the stress level decreases. Cycles to failure data were more scattered at low stress levels.
2. The positive proportional relationship between strength/hardness and fatigue life was repeatedly revealed in this study.
3. For hand-forged samples at T6 temper, T direction performed better than S direction in fatigue life ($N_T > N_S$); at T8-8% temper, T direction performed better than S direction, and both performed better than ST45 direction ($N_T > N_S > N_{ST45}$); at T8-4% temper, T direction performed better than ST45 direction ($N_T > N_{ST45}$).
4. It appeared that T8 temper did not experience worse anisotropic behavior compared to T6 temper for hand-forged samples.
5. For hand-forged samples, T8-8% strain and T8-4% strain showed similar fatigue life at median and low stress levels, while T8-4% had much better fatigue life at high stress levels. Both T8 tempers had longer fatigue life than the T6 tempers. In general, aircraft wheel specimens at T8 temper, with higher yield and tensile strength, showed better fatigue life than at T6 temper. A positive correlation is observed between the hardness and the fatigue life.
6. It appeared that different locations on an aircraft wheel could experience huge differences in fatigue life, especially at low stress levels. The tubewell location experienced more hot work. As a result, samples at tubewell location have longer fatigue life.
7. It appeared that aircraft wheel samples had better fatigue life compared with hand-forged samples. Die forging, with more percent hot work, produced finer grains.
8. Taken from the same type of aircraft wheel, AA2195 specimens showed better fatigue life than AA2014 specimens. The addition of Li appeared to improve both strength and fatigue life.
9. Forging, being more random and multi-directional in deformation (hot work), seems to have less anisotropy compared to rolling and extrusion in one direction.

Acknowledgments

The authors highly acknowledge and thank Mr. Ye Thura Hein (Loyola Marymount University) for his help in revising and editing the manuscript.

References

1. N. Nayan, N.P. Gurao, S.V.S. Narayana Murty, A.K. Jha, B. Pant, S.C. Sharma, and K.M. George, Microstructure and Micro-texture Evolution During Large Strain Deformation of an Aluminum–Copper–Lithium Alloy AA 2195, *Mater. Des.*, 2015, **65**, p 862–868
2. N. Jiang, G. Xiang, and Z.Q. Zheng, Microstructure Evolution of Aluminum–Lithium Alloy 2195 Undergoing Commercial Production, *Trans. Nonferrous Met. Soc. China*, 2010, **20**(5), p 740–745
3. N. Nayan, S.V.S. Narayana Murty, A.K. Jha, B. Pant, S.C. Sharma, K.M. George, and G.V.S. Sastry, Processing and Characterization of Al-Cu-Li Alloy AA2195 Undergoing Scale Up Production Through the Vacuum Induction Melting Technique, *Mater. Sci. Eng. A*, 2013, **576**, p 21–28
4. Z.X. Zhu, J. Han, C. Gao, M. Liu, J.W. Song, Z.W. Wang, and H.J. Li, Microstructures and Mechanical Properties of Al-Li 2198-T8 Alloys Processed by Two Different Severe Plastic Deformation Methods: A Comparative Study, *Mater. Sci. Eng. A*, 2017, **681**, p 65–73
5. A. Hekmat-Ardakan, E.M. Elgallad, F. Ajersch, and X.G. Chen, Microstructural Evolution and Mechanical Properties of As-Cast and T6-Treated AA2195 DC Cast Alloy, *Mater. Sci. Eng. A*, 2012, **558**, p 76–81
6. L. Wang, M. Hao, G.A. Li, and G.H. Chen, In-situ Investigation of the Fracture Behaviors of 2195-T8 Aluminum-Lithium Alloy, in *MATEC Web Conference*, vol 67(05028) (2016), p 1–6
7. A.A. El-Aty, Y. Xu, X.Z. Guo, S.H. Zhang, Y. Ma, and D.Y. Chen, Strengthening Mechanisms, Deformation Behavior, and Anisotropic Mechanical Properties of Al-Li Alloys: A Review, *J. Adv. Res.*, 2017, **10**, p 49–67
8. N. Nayan, S.V.S. Narayana Murty, A.K. Jha, B. Pant, S.C. Sharma, K.M. George, and G.V.S. Sastry, Mechanical Properties of Aluminum–Copper–Lithium Alloy AA2195 at Cryogenic Temperatures, *Mater. Des.*, 2014, **58**, p 445–450
9. W.T. Wu, Z.Y. Liu, S. Bai, F.D. Li, M. Liu, and A. Wang, Anisotropy in Fatigue Crack Propagation Behavior of Al-Cu-Li Alloy Thick Plate, *Mater. Charact.*, 2017, **131**, p 440–449
10. J. Chen, Q.L. Pan, X.H. Yu, M.J. Li, H. Zou, H. Xiang, Z.Q. Huang, and Q. Hu, Effect of Annealing Treatment on Microstructure and Fatigue Crack Growth Behavior of Al-Zn-Mg-Sc-Zr Alloy, *J. Cent. South Univ.*, 2018, **25**(5), p 961–975
11. H. Aydin, M. Tutar, A. Durmuş, A. Bayram, and T. Sayaca, Effect of Welding Parameters on Tensile Properties and Fatigue Behavior of Friction Stir Welded 2014-T6 Aluminum Alloy, *Trans. Indian Inst. Met.*, 2012, **65**(1), p 21–30
12. Q.B. Yang, X.Z. Wang, X. Li, Z.H. Deng, Z.H. Jia, Z.Q. Zhang, G.J. Huang, and Q. Liu, Hot Deformation Behavior and Microstructure of AA2195 Alloy Under Plane Strain Compression, *Mater. Charact.*, 2017, **131**, p 500–507
13. Z.W. Chen, K. Zhao, and L. Fan, Combinative Hardening Effects of Precipitation in a Commercial Aged Al-Cu-Li-X Alloy, *Mater. Sci. Eng. A*, 2013, **588**, p 59–64
14. A. Medjahed, A. Henniche, M. Derradji, T.F. Yu, Y. Wang, R.Z. Wu, L.G. Hou, J.H. Zhang, X.L. Li, and M.L. Zhang, Effects of Cu/Mg Ratio on the Microstructure, Mechanical and Corrosion Properties of Al-Li-Cu-Mg-X Alloys, *Mater. Sci. Eng. A*, 2018, **718**, p 241–249
15. J.F. Li, Z.H. Ye, D.Y. Liu, Y.L. Chen, X.H. Zhang, X.Z. Xu, and Z.Q. Zheng, Influence of Pre-deformation on Aging Precipitation Behavior of Three Al-Cu-Li Alloys, *Acta Metall. Sin. (Engl. Lett.)*, 2017, **30**(2), p 33–145
16. J.H. Kim, J.H. Jeun, H.J. Chun, Y.R. Lee, J.T. Yoo, J.H. Yoon, and H.S. Lee, Effect of Precipitates on Mechanical Properties of AA2195, *J. Alloys Compd.*, 2016, **669**, p 187–198
17. O.S. Es-Said, C.J. Parrish, C.A. Bradberry, J.Y. Hassoun, R.A. Parish, A. Nash, and N.C. Smythe, Effect of Stretch Orientation and Rolling Orientation on the Mechanical Properties of 2195 Al-Cu-Li Alloy, *J. Mater. Eng. Perform.*, 2011, **20**(7), p 1171–1179
18. H.Y. Li, D.S. Huang, W. Kang, J.J. Liu, Y.X. Ou, and D.W. Li, Effect of Different Aging Processes on the Microstructure and Mechanical Properties of a Novel Al-Cu-Li Alloy, *J. Mater. Sci. Technol.*, 2016, **32**(10), p 1049–1053
19. M.C. Chaturvedi and D.L. Chen, Effect of Specimen Orientation and Welding on the Fracture and Fatigue Properties of 2195 Al-Li Alloy, *Mater. Sci. Eng. A*, 2004, **387**, p 465–469

20. P. Khanikar, Y. Liu, and M.A. Zikry, Experimental and Computational Investigation of the Dynamic Behavior of Al-Cu-Li Alloys, *Mater. Sci. Eng. A*, 2014, **604**, p 67–77
21. A. Wang, Z.Y. Liu, M. Liu, W.T. Wu, S. Bai, and R.X. Yang, Texture and Tempered Condition Combined Effects on Fatigue Behavior in an Al-Cu-Li Alloy, *J. Mater. Eng. Perform.*, 2017, **26**(6), p 2453–2458
22. R.J. Rioja and J. Liu, The Evolution of Al-Li Base Products for Aerospace and Space Applications, *Metall. Mater. Trans. A*, 2012, **43**(9), p 3325–3337
23. T. Dorin, A. Deschamps, F.D. Geuser, and F. Robaut, Impact of Grain Microstructure on the Heterogeneity of Precipitation Strengthening in an Al-Li-Cu Alloy, *Mater. Sci. Eng. A*, 2015, **627**, p 51–55
24. R. Crooks, Z. Wang, V.I. Levit, and R.N. Shenoy, Micro-texture, Microstructure and Plastic Anisotropy of AA2195, *Mater. Sci. Eng. A*, 1998, **257**(1), p 145–152
25. ISO 1143, *Metals—Rotating Bar Bending Fatigue Testing*, 1975
26. Weber Metals, Inc., Paramount, CA. http://web.webermetals.com/. Accessed June 2018
27. L.P. Xu, Q.Y. Wang, and M. Zhou, Micro-crack Initiation and Propagation in a High Strength Aluminum Alloy During Very High Cycle Fatigue, *Mater. Sci. Eng. A*, 2018, **715**, p 404–413
28. D.R. Askeland, P.P. Fulay, and W.J. Wright, The science and engineering of materials, 6th edn. *Cengage Learning* (2011), p 266–284. **(Print)**
29. D.D. Tian, X.S. Liu, G.Q. He, Y. Shen, S.Q. Lv, and Q.G. Wang, Low Cycle Fatigue Behavior of Casting A319 Alloy Under Two Different Aging Conditions, *Mater. Sci. Eng. A*, 2016, **654**, p 60–68
30. F. Alzubi, M. Timko, Y. Li, R. Toal, K. Tovalin, and O.S. Es-Said, Large Versus Small Grain Sizes on Fatigue Life of Aluminum Aircraft Wheels, *Defect Diffus. Forum*, 2019, **391**, p 174–194
31. P.S. De, R.S. Mishra, and J.A. Baumann, Characterization of High Cycle Fatigue Behavior of a New Generation Aluminum Lithium Alloy, *Acta Mater.*, 2011, **59**(15), p 5946–5960
32. N.J. Kim and E.W. Lee, Effect of T1 Precipitate on the Anisotropy of Al-Li Alloy 2090, *Acta Metall. Mater.*, 1993, **41**(3), p 941–948
33. M. Gazizov and R. Kaibyshev, High Cyclic Fatigue Performance of Al-Cu-Mg-Ag Alloy Under T6 and T840 Conditions, *Trans. Nonferrous Met. Soc. China*, 2017, **27**(6), p 1215–1223
34. Q.K. Xia, Z.Y. Liu, and H. Wang, Fatigue Property of 2A12 Aluminum Alloy for T6 and T8 Aging, *Trans. Mater. Heat Treat.*, 2014, **35**(4), p 67–71
35. B.I. Rodgers and P.B. Prangnell, Quantification of the Influence of Increased Pre-stretching on Microstructure–Strength Relationships in the Al-Cu-Li Alloy AA2195, *Acta Mater.*, 2016, **108**, p 55–67
36. Y.X. Wang, G.Q. Zhao, X. Xu, X.X. Chen, and W.D. Zhang, Microstructures and Mechanical Properties of Spray Deposited 2195 Al-Cu-Li Alloy Through Thermo-Mechanical Processing, *Mater. Sci. Eng. A*, 2018, **727**, p 78–89
37. C. Laird and G.C. Smith, Crack Propagation in High Stress Fatigue, *Philos. Mag.*, 1962, **7**(77), p 847–857
38. T. Kermanidis, A.D. Zervaki, V. Modas, A.N. Chamos, and S.G. Pantelakis, Fatigue Performance of Pre-corroded 6xxx Aluminum Alloy Laser Beam Welds With Dissimilar Heat Treatment, *Procedia Eng.*, 2014, **74**, p 22–26